ELSEVIER

Solid State Ionics 145 (2001) 275–294

SOLID STATE IONICS

www.elsevier.com/locate/ssi

Structural phase transitions, oxygen vacancy ordering and protonation in doped $BaCeO_3$: results from time-of-flight neutron powder diffraction investigations

K.S. Knight *

ISIS Facility, Rutherford Appleton Laboratory, Chilton, Didcot, Oxon OX11 0QX, UK

Received 25 September 2000; received in revised form 28 December 2000; accepted 25 January 2001

Abstract

The structural crystallography of the mixed-ion conductor $BaCe_{1-x}Ln_xO_{3-\delta}$ and the parent compound $BaCeO_3$ are reviewed from the perspective of neutron powder diffraction results. High-resolution, time-of-flight, powder diffraction has been used to verify the unit cell metric, and to correct the setting of this metric to the space group for both the undoped phase and for Y- and Nd-doped material. Key superlattice reflections are utilised to disprove the structural phase transitions inferred from Raman spectroscopy in temperature and Nd dopant concentration, with high-resolution powder diffraction showing the correct crystal symmetries in both cases. Crystal structure refinements have shown that negligible perturbation of the parent compound structure occurs on Y- and Nd-doping, and the extrinsic vacancy was found to be ordered on one of the two crystallographically independent oxygen atoms. A possible structural site for the proton has been proposed from measurements made at low temperatures and the potential for more detailed neutron diffraction studies is discussed.

Keywords: Barium cerate; Neutron diffraction; Crystal structure; Phase transitions

1. Introduction

The ionic properties of doped barium cerate perovskites have been well-established for over a decade since the pioneering work of Iwahara et al., and the subject has been recently reviewed by Bonanos et al. [1 and references therein]. The characterisation of the compound in terms of the more basic physical properties of structure and dynamics has unfortunately lagged behind in the drive to make useful solid-state electrochemical devices. In this review, we aim to place the structural aspects of the materials that have been studied so far on to a firm footing. The heavy atoms in $BaCeO_3$ occupy sites of high pseudosymmetry, thus making detailed, accurate structural refinements all but impossible with X-ray diffraction. By contrast, the sensitivity of neutron diffraction to both the light atom positions and site occupancies have made the technique invaluable in the structural characterisation of this compound. This article reviews the results from time-of-flight neutron diffraction measurements made on both the undoped and the doped phase as a function of doping level and temperature.

* Department of Mineralogy, Natural History Museum, Cromwell Road, London SW7 5BD, UK.

E-mail address: ksk@isise.rl.ac.uk (K.S. Knight).

0167-2738/01/$ - see front matter
PII: S0167-2738(01)00952-3

The article begins with a basic review of the aristotype structure and the distortions that are frequently observed in the perovskite family. Glazer's [5,6] classification is introduced and related to the important zone boundary modes that give rise to the tilting of the octahedra. Superlattice reflections that arise from the condensation of one or more of these modes are then used to show the advantages of neutron diffraction over X-ray diffraction in the structural characterisation of $BaCeO_3$. The ambient temperature crystal structure and the problem of determining the correct metric and space group are then reviewed, before the effects of doping and the possible phase transitions that doping may induce are considered. The high-temperature behaviour has long been regarded as contentious, and high- and medium-resolution neutron diffraction data are presented to show the correct phase transition sequence in both $BaCeO_3$ and with Y and Nd dopants. Low temperature neutron diffraction measurements on undoped and Y-doped $BaCeO_3$ have been used to derive a possible site for the incorporated structural proton, and improvements to this experimental determination are suggested. Finally, some of the remaining questions that neutron diffraction may be able to solve are outlined in the last section.

Although this article draws from results made using time-of-flight neutron powder diffraction instruments, most, if not all conclusions deduced from the data collected could have been as easily measured using reactor-based instrumentation.

2. Perovskite crystallography

The aristotype perovskite structure with stoichiometry ABC_3 is cubic, with space group $Pm\bar{3}m$ and consists of infinite, three-dimensional, corner-sharing BC_6 octahedra with a dodecahedrally coordinated *A*-site in the centre of a cavity generated by eight surrounding octahedra. In the aristotype, the *A*-site forms the centre of a cube with the *B*-site cations at each of the eight corners as shown in Fig. 1. However, this ideal structure is rarely achieved at ambient temperature due to the strict constraints placed on the $A-C$ and $B-C$ bond lengths, which would be required to be in the ratio of $\sqrt{2}$:1, and furthermore, all of the individual $A-C$ and $B-C$ bond lengths would be required to be equal. To avoid this rigid constraint, most perovskites consequently show distortions from the aristotype phase, resulting in what are generally termed hettotype phases. The distortions from the aristotype phase can be classified in terms of four mechanisms, distortions of the BC_6 octahedra, displacement of the *B*-site cation within the octahedron, displacement of the *A*-site cation and rotations of the octahedra relative to one another. The first mechanism has been ob-

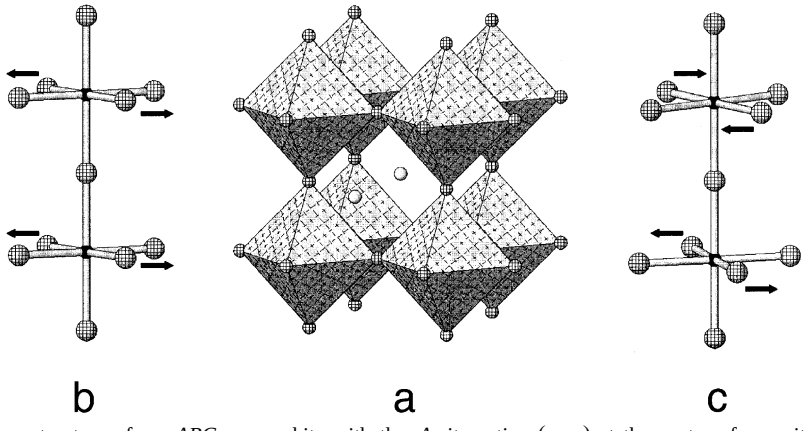

Fig. 1. (a) The aristotype structure of an ABC_3 perovskite with the *A*-site cation (grey) at the centre of a cavity surrounded by eight, corner-sharing BC_6 octahedra. (b) The *M*-point mode, M_3, showing the in-phase tilting of neighbouring octahedra along a cubic four-fold axis. (c) The *R*-point mode, R_{25}, showing the antiphase tilting of neighbouring octahedra along a cubic four-fold axis.

served in the Jahn–Teller distortion of the Cu^{2+} ion in $KCuF_3$, the second and third are characteristics of ferroelectric distortions in, for example, $BaTiO_3$ in the former and lead-based relaxor phases in the latter, but the most common, and indeed relevant to this review of $BaCeO_3$, is the fourth. Tilting of the octahedra is typically observed when the *A* cation is too small for the dodecahedral site, and allows shortening of *A*–*C* bonds, while maintaining the *B*–*C* first coordination shell distances. This effect can be appreciated by comparing the magnitudes of the tilts in the alkaline earth cerate perovskites. $SrCeO_3$, for which the ionic radius of Sr^{2+} in eight-fold coordination is 1.26 Å, exhibits an in-phase tilt of 11° and an antiphase tilt of 12.5° (for explanation of these terms, see below). The larger Ba^{2+} ion with an identical coordination number in $BaCeO_3$, has a larger ionic radius of 1.42 Å, and consequently exhibits smaller tilts of 6° and 8.8° for the in-phase and antiphase rotations, respectively.

Glazer [5,6], building on the earlier perovskite structural work of Megaw [2], and using both the concept of soft-modes developed by Cochran [3] and the normal mode analysis of the perovskite structure by Cowley [4], produced two seminal papers on the classification and characterisation of perovskites with tilted octahedra. Glazer considered the lowering of symmetry from the aristotype phase caused by the tilting of layers of octahedra around the four-fold axes of the cubic structure. The tilting of successive octahedra along this axis can be achieved in one of two ways: either the layers rotate in the same sense as the first or in the opposite sense. Glazer introduced a convenient notation for the description of the structures derived from these successive tilts. Each system of tilts was designated by the symbol $a^i b^j c^k$, where *abc* represented the magnitude of the rotations around each pseudocubic axis and the letters, indicating the equality or inequality of the magnitudes of these rotations. The superscripts relate to the sense of the tilt of successive octahedra along the rotation axis, $+$, indicating the same sense, $-$, indicating the opposite sense. The superscript 0 represents no tilt around a particular pseudocubic direction. For example, the system $a^-a^-a^-$ represents three equal antiphase tilts around the pseudocubic directions and is the tilt system for $BaCeO_3$ between 673 and 1173 K, $a^0b^-b^-$ represents two antiphase tilts of equal magnitude and is the tilt system for $BaCeO_3$ between 563 and 673 K. The most common tilt system is represented by $a^+b^-b^-$ [6], a single in-phase tilt and two antiphase tilts of equal magnitude, and represents the tilt system of $BaCeO_3$ between 4.2 and 563 K. The aristotype phase is $a^0a^0a^0$. In his analysis, Glazer found 23 independent tilt systems and published both the derived space groups and the relationship between the aristotype unit cell and the new crystallographic unit cells. As only rotations of successive octahedra were considered by Glazer, leading to at most, a doubling of the unit cell edges with respect to the aristotype phase, these perovskite hettotypes are often termed bipartite.

The effect of tilting on the powder diffraction pattern of a perovskite is two-fold with the lowering of symmetry (i) splitting the fundamental reflections, i.e. those that can be approximately indexed on the reciprocal lattice of the (possibly hypothetical) aristotype phase, and (ii) the development of superlattice reflections between the fundamental reflections.

What is frequently forgotten in purely structural studies of perovskites is the intimate relationship between Glazer's notation and the underlying lattice dynamics in the perovskite structure. Many, if not most, bipartite perovskites undergo phase transitions in which the octahedral tilts are gained or lost as a function of temperature, pressure, or possibly composition in solid solutions. In most compounds, these changes are caused by the condensation of one or more soft-modes at the *R*- and/or *M*-points of the pseudocubic Brillouin zone. The mode at the *R*-point has wave vector $1/2\mathbf{a}^* + 1/2\mathbf{b}^* + 1/2\mathbf{c}^*$, is triply degenerate and has the effect of rotating successive octahedra in an antiphase manner, i.e. $a-$ tilt in Glazer's notation. This mode is frequently termed either the R_{25} or R_4^+ mode but in all subsequent discussions, it will simply be termed the *R*-point mode for brevity. The mode at the *M*-point has wave vector $1/2\mathbf{a}^* + 1/2\mathbf{b}^*$ or symmetry-related positions, is a singlet and has the effect of rotating successive octahedra in an in-phase manner, i.e. $a+$ tilt in Glazer's notation. This mode is frequently termed either the M_3 or M_3^+ mode but again for brevity, and as there is no ambiguity in the analysis to follow, it will simply be termed the *M*-point mode. The effect of these two modes is shown diagrammatically in Fig. 1. If one or more of these

modes condense at a phase transition, then the associated point in the Brillouin zone will become a reciprocal lattice vector in the new phase. It is therefore possible to characterise the superlattice reflections that occur in the diffraction pattern of a perovskite as being derived from a specific tilt type. This becomes an important aid when attempting to determine which is the true space group of a new phase or compound.

Recently, Woodward [7] and Howard and Stokes [8] have re-evaluated Glazer's work and deduced that the number of independent tilt systems was less than 23. Using group theoretical arguments, Howard and Stokes have shown that there are only 15 space groups consistent with condensation at the *M*- and/or *R*-points and have presented in diagrammatic form, the group–subgroup relationship between the possible space groups. The thermodynamic order for structural phase transitions between possible pairs of space groups was also derived on the basis of the Landau theory [9]. This theory states that second order phase transitions are only permissible between two space groups exhibiting a group–subgroup relationship, and if such a relationship does not exist, then the phase transition must be first order. We shall appeal to this result in the discussion of the high-temperature behaviour of $BaCeO_3$.

When carrying out the initial X-ray structural investigation of a perovskite phase, it is important to bear in mind two main points; the first is that if the tilts are small, the splitting of the fundamental reflections will be small, and secondly, that superlattice reflections are generally much weaker than the fundamental reflections. The first can normally be dealt with by measuring the data at the highest resolution achievable, and it is possible that focussing cameras may be preferable to step-scan diffractometers in this respect. In addition, even if the data do not show line splitting, there are benefits to carrying out systematic diffraction peak width analysis, and using, for example, Williamson–Hall plots to determine the true nature of the unit cell metric. The second point is more difficult, especially if the compound contains heavy atoms in sites of high pseudosymmetry. In this case, data collection strategies for step-scan diffractometers need to be modified to significantly spend more time scanning over the potential superlattice reflections at potential *R*- and *M*-point positions than at fundamental reflection positions. The few laboratory X-ray Rietveld refinements of the cerate perovskites that have been published all show poor estimated standard deviations on the oxygen coordinates, mainly because these superlattice peaks, which are almost vanishingly weak, have been poorly determined.

The weakness of superlattice reflections for oxide systems arise principally from the fact that scattering cross-sections for X-rays are proportional to the

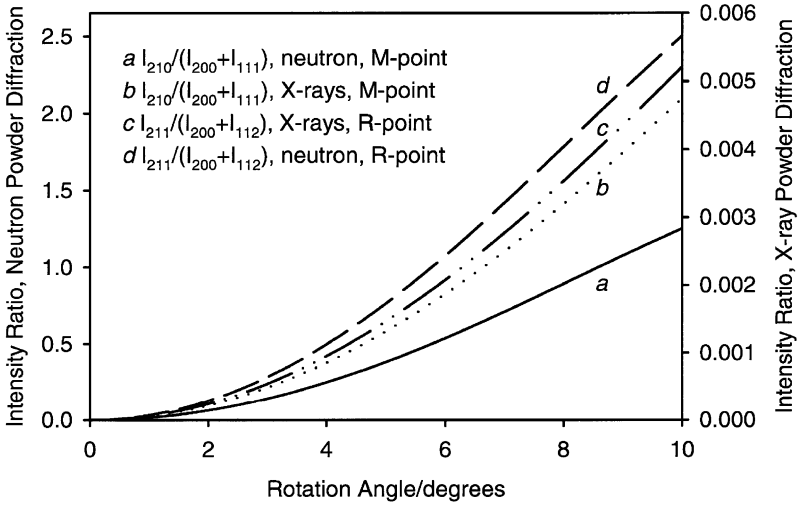

Fig. 2. The variation of the intensity ratio of *M*- and *R*-point superlattice reflections to a fundamental reflection as a function of octahedron tilt angle for two hypothetical structures of $BaCeO_3$ in space groups $P4/mbm$ and $I4/mcm$, respectively.

square of the atomic number. For oxygen, the scattering cross-section is often significantly smaller than the equivalent for the cations. Furthermore, if we consider a single *R*- or *M*-point condensation, in space groups $I4/mcm$ $(a^0a^0c^-)$ and $P4/mbm$ $(a^0a^0c^+)$, respectively, the structure factors associated with the superlattice reflections are derived only from a subset of the oxygen atoms. By contrast, neutron scattering lengths have no simple atomic number dependence, and in the case of $BaCeO_3$, oxygen has the largest scattering cross-section of the three constituent elements. As a result, superlattice reflections are often considerable for neutron diffraction, thus making space group assignment a significantly easier task than by using X-rays.

As an example of the superior visibility of superlattice reflections with neutron diffraction than with X-ray diffraction, the intensity ratio of a typical *M*- and *R*-point reflection to a neighbouring fundamental reflection has been calculated as a function of octahedral rotation angle for $BaCeO_3$ using the hypothetical space groups $I4/mcm$ and $P4/mbm$. If a cubic perovskite undergoes a phase transition arising from a soft-mode condensing at the *R*-point, then the fundamental 110 reflection becomes split in the new tetragonal phase (space group $I4/mcm$) with new indices 200 and 112, and with an approximate intensity ratio of 1:2. A superlattice reflection should be observed with index 211. If a cubic perovskite undergoes a phase transition arising from a soft-mode condensing at the *M*-point, then the fundamental 110 reflection becomes split in the new tetragonal phase (space group $P4/mbm$) with new indices 200 and 111, and also with an approximate intensity ratio of 1:2. A superlattice reflection should be observed with index 210. Fig. 2 shows the ratio of the 211 superlattice reflection to the neighbouring 200/112 and the 210 superlattice reflection to the 200/111 reflections. For ease of computation, the mean square displacements have been ignored and set to zero.

It is clear from this figure that in the case of neutron diffraction, it is possible for the intensity of the superlattice reflections to even exceed the sum of the intensities of these particular fundamental reflections; however, for X-rays, the maximum intensity ratio is well below 0.5% for most of the rotation angle range. In addition, it should be noted that the superlattice intensity ratio increases with the magnitude of the octahedral rotation. The strength of the superlattice reflections from neutron powder diffraction data therefore allows precise structural models to be determined using the Rietveld method even in the vicinity of phase transitions. By way of illustration of the difficulty of achieving precise structural models of doped $BaCeO_3$, Knight et al. [10] failed to determine a sensible room temperature structural model for $BaCe_{0.9}Gd_{0.1}O_{2.95}$ even when using both the high-resolution and high-flux afforded by synchrotron radiation powder diffraction.

The significant improvement in the information content of a neutron powder diffraction pattern is highlighted further when the whole pattern is considered. Fig. 3 shows simulated powder diffraction patterns from orthorhombic $BaCeO_3$ for both X-rays and neutrons at a wavelength of 1.54 Å, based on the room temperature structural model of Knight and Bonanos [11]. The simulation not only illustrates the paucity of information on the superlattice intensity variations in the X-ray pattern, but also the addi-

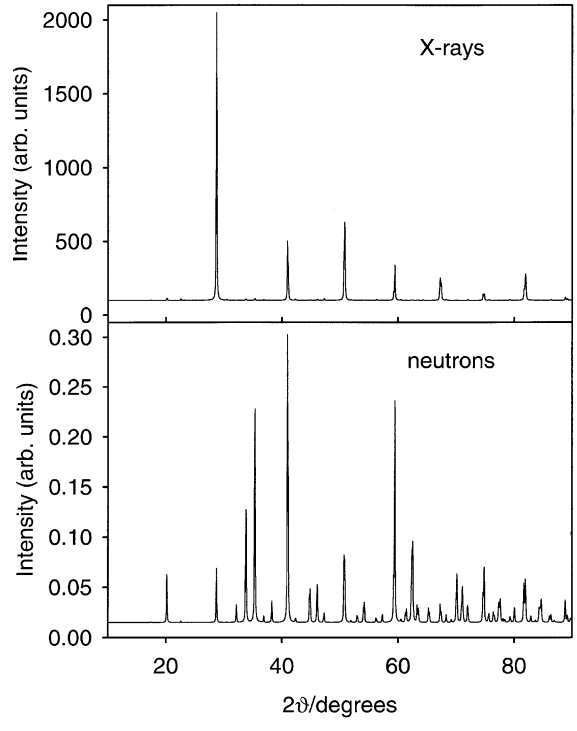

Fig. 3. Simulations of the X-ray and neutron diffraction patterns of $BaCeO_3$ at a wavelength of 1.54 Å based on the room temperature structural model of Knight and Bonanos [11].

tional advantage of neutron diffraction, which is the lack of form-factor fall off with Q ($Q = 4\pi \sin\theta/\lambda$). The neutron powder pattern clearly shows the visibility of the superlattice peaks throughout the pattern even up to high values of Q.

The arguments developed above will be used to illustrate the characterisation of $BaCeO_3$, the effect of doping in the material, the structural phase transitions as a function of temperature, and a possible structural site for the proton.

3. Ambient temperature crystal system, unit cell metric, space group and crystal structure

Common to many perovskites, the crystal system, unit cell metric and space group of $BaCeO_3$ has 'evolved' in time as instrumentation has improved and alternative radiation probes to X-rays have been employed to study the material. Early work, employing X-ray powder photography, with insufficient resolution to determine the splitting of the fundamental reflections and insufficient flux to observe the superlattice reflections, found the compound to be cubic at room temperature [12–16]. Later work by Preda and Dinescu [17] suggested that it was tetragonal at room temperature with a phase transition to cubic at ~ 700 K. In his systematic study of ABO_3 compounds in 1957, Roth [18] found the compound to be pseudocubic, possibly orthorhombic, and this was subsequently confirmed by Danelon Mastromonaco et al. [19]. In this study, the lattice parameters were determined as being of the type $2a\sqrt{2}a\sqrt{2}a$, where a is the aristotype lattice parameter, but no potential space group was proposed. Later work using both X-rays [20] and neutron powder diffraction [21] confirmed the compound to be orthorhombic, with the neutron pattern indicating the space group to be *Pbnm*, $a^-a^-c^+$, (space group No. 62) with lattice parameters $a = 6.212(1)$ Å, $b = 6.235(1)$ Å and $c = 8.781(1)$ Å. A structural model for $BaCeO_3$ was derived by pattern decomposition of the neutron powder data. Despite a good fit to the neutron diffraction data, suggesting that the cell and space group were in fact correct, Longo et al. [22] suggested that the unit cell was in error and that the true crystal system was tetragonal with a metric of $a = 6.212(2)$ Å and $c = 8.804(4)$ Å. Knight et al. [10] investigated the crystal system, unit cell metric controversy with a sample of $BaCe_{0.9}Y_{0.1}O_{2.95}$ using the high-resolution, time-of-flight, powder diffractometer HRPD at the ISIS spallation neutron source. This instrument which has a resolution of $\Delta d/d = 8 \times 10^{-4}$ and a resolution function that is essentially independent of Q, provided data that was analysed using model-independent (Pawley) fitting [23] as no structural model was proposed for the Longo revised cell. Although this technique disproved the cell of Longo, $\chi^2 = 3.8$ for a fit in the Laue group $P4/mmm$, Knight et al. unfortunately chose to compare this result with the orthorhombic Laue group *Pmmm*, for which $\chi^2 = 1.1$, rather than make the comparison with a fit in the space group *Pbnm* used by Jacobson et al. [21] in the structural work. The model-free fit confirmed the unit cell metric of Danelon Mastromonaco but did not confirm the setting of the space group to the unit cell metric. On the basis of this confirmation, Knight et al. published the first crystal structure refinements of Y- and Gd-doped $BaCeO_3$ but chose an alternative setting of space group No. 62, *Pmcn*, ($a^+b^-b^-$, axial setting $2a\sqrt{2}a\sqrt{2}a$), for their work. These data were collected on the high-flux, medium-resolution, time-of-flight diffractometer POLARIS at ISIS.

The first evidence that something was in error became apparent when data collected on undoped $BaCeO_3$ were being analysed. Detector improvements on the POLARIS diffractometer in the intervening period had lead to an increase in count-rate of a factor of three with concomitant improvements in the statistical quality of the data, especially at long times-of-flight, corresponding to the longer d-spacing reflections. Rietveld refinement of the significantly improved data apparently required the two short axes to be interchanged from the results of the Pawley refinement from HRPD. As the resolution of this instrument ($\Delta d/d = 5 \times 10^{-3}$) was insufficient to resolve either the splitting of the fundamental reflections or the superlattice reflections, a data set was collected on HRPD and this time was fitted using the Pawley method in the space group *Pmcn*. No significant difference from the fit in *Pmmm* was found for the whole pattern with the exception of a single group of weak M-point superlattice reflections shown in Fig. 4. The upper left-hand side of the figure shows the results of the Pawley refinement for

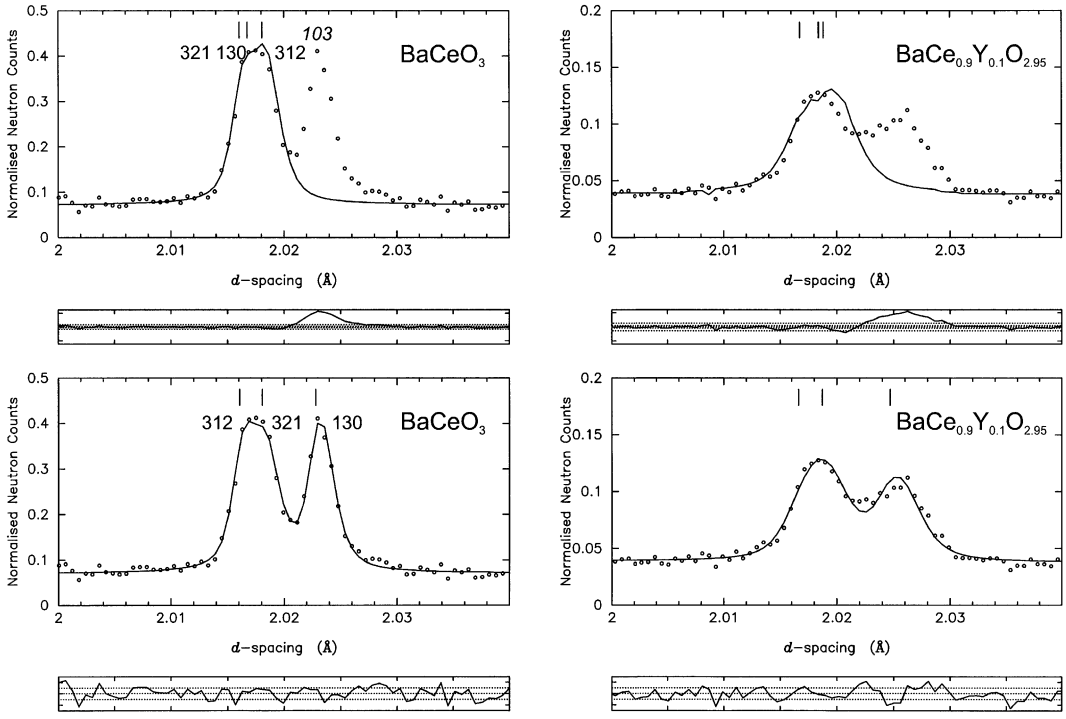

Fig. 4. Diagnostic regions of the diffraction pattern of $BaCeO_3$ and $BaCe_{0.9}Y_{0.1}O_{2.95}$ fitted using the Pawley [23] method. The upper left-hand side shows the unfitted systematic absence reflection, 103, for the axial setting of Jacobson et al. transformed to space group *Pmcn*. The lower left-hand side shows the correct setting of the axial metric for this space group obtained by reversing the *b* and *c* axes. The upper and lower right-hand side of the figure shows data from the identical group of reflections for $BaCe_{0.9}Y_{0.1}O_{2.95}$. The upper diagram shows the incorrect recent revision of the cell by Münch et al. [25], which shows the unfitted 103 reflection. The lower diagram is the fit according to the correct cell setting of Knight and Bonanos [11] as for the case of $BaCeO_3$. In all four figures, the dotted lines correspond to $\Delta/\sigma = \pm 3$.

the setting originally published by Knight et al. [10], and the lower left-hand side with the *b* and *c* axes are reversed. It is clear that in the upper diagram, there is an unfitted reflection that is consistent with the unit cell metric, all the data were fittable in the Laue group *Pmmm*, but is not consistent with the systematic absence conditions of space group *Pmcn*. This reflection indexes as 103 on this unit cell metric, which is a systematic absence by virtue of the *c*-glide plane perpendicular to the *b* axis ($h0l$, $l = 2n + 1$, absent). On reversing the unit cell metric, all reflections are fitted and this reflection now indexes as 130, which is permitted by the *n*-glide plane perpendicular to the *c* axis ($hk0$, $h + k = 2n + 1$, absent). The consistent metric for space group *Pmcn* was found to be $a = 8.77693(4)$ Å, $b = 6.23571(3)$ Å and $c = 6.21612(4)$ Å. In a subsequent publication, Knight and Bonanos [24] reported the error and the correction to the lattice metric and space group. The crystal structures of the two doped phases were re-refined with the consistent cell and space group [24], and in a further publication, Knight and Bonanos [11] reported the crystal structure for the undoped phase and with 15 mol% Pr-doping.

Recently, Münch et al. [25] have published crystal structure refinements of $BaCe_{0.9}Y_{0.1}O_{2.95}$ using laboratory-source X-ray diffraction. Despite estimated standard deviations which are well in excess of an order of magnitude poorer than those derived by Knight and Bonanos [24] for the oxygen coordinates, these authors claimed that their data only gave a satisfactory model if the axes were transformed back to the original setting of Jacobson et al. [10,21]. Although it is difficult to give credence to structures

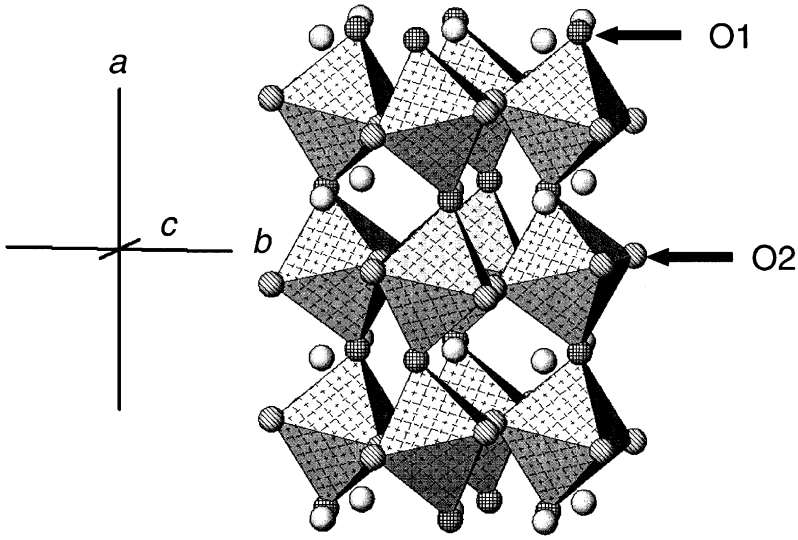

Fig. 5. The crystal structure of $BaCeO_3$ at room temperature based on the structure of Knight and Bonanos [11], orthorhombic, space group *Pmcn*. The crystallographically independent oxygen atoms are indicated by arrows. O_1 lies on the mirror plane in the structure, O_2 lies on the general site.

of doped $BaCeO_3$ derived from both laboratory X-rays and low-resolution instrumentation for the reasons outlined earlier in this review, later we shall show that their revised axial setting is in fact incorrect. The right-hand side of Fig. 4 shows part of the Pawley refinement of $BaCe_{0.9}Y_{0.1}O_{2.95}$ at room temperature from neutron powder diffraction data collected on HRPD. The upper right-hand side shows the setting of Münch et al., the lower right-hand side, the setting of Knight et al. As in the case of $BaCeO_3$, we observe the 103 reflection in the *Pmcn* setting of Münch et al. for the $BaCe_{0.9}Y_{0.1}O_{2.95}$ data, which, as pointed out above, is a systematically absent reflection. The bottom right-hand side shows the fit in the setting of Knight et al. where all peaks are accounted for, conclusively disproving the assertion of Münch et al. that the short axes need reversing in $BaCe_{0.9}Y_{0.1}O_{2.95}$. In a systematic study of $BaCe_{1-x}Nd_xO_{3-\delta}$, to be described in detail below, we find the identical axial setting of the space group as in $BaCeO_3$ and $BaCe_{0.9}Y_{0.1}O_{2.95}$, and furthermore, we can find no compelling crystal–chemical argument on why this setting should not apply to all rare-earth dopants in $BaCeO_3$.

The positions of the two independent oxygen atoms in the crystal structure of $BaCeO_3$ are shown in Fig. 5. The CeO_6 octahedron is very regular with an average bond length of 2.240 Å, a volume of 14.974 $Å^3$, a quadratic elongation of 1.000415 and an octahedral angle variance of $1.309^{\circ 2}$. The Ba occupies an 8-coordinated site with an average bond length of 2.931 Å and shows a significant displacement in the *c* direction, with a much smaller displacement in *b*. The magnitudes of the tilts are 6° and 8.8° for the *M*- and *R*-point rotations, respectively. The crystal structure refined from POLARIS data shows no major changes in the structure from that originally determined by Jacobson et al. [21].

Transformations from the space group *Pmcn* to the standard setting of the space group, *Pnma*, are given in Appendix A1 of this paper.

4. The effects of doping on the crystal structure and dopant-induced phase transitions

The crystal structure refinements of $BaCe_{0.9}Gd_{0.1}O_{2.95}$, $BaCe_{0.9}Y_{0.1}O_{2.95}$ and $BaCeO_3$ showed that the effect of doping on the crystal structure was minimal; however, Knight and Bonanos found that the extrinsic vacancy, introduced on Y-doping was localised only on the oxygen atom in general posi-

tions. Due to the extreme absorption cross-section of Gd to thermal neutrons, it was not possible to derive anything other than a very rough structural model for $BaCe_{0.9}Gd_{0.1}O_{2.95}$ because at the time the neutron data were collected, Rietveld codes that were capable of the co-refinement of neutron time-of-flight and synchrotron X-ray data were not readily available. In the intervening period between the first crystal structures being reported [10] and the subsequent corrections that were made using the correct metric and space group [24], Raman spectroscopy had been used to infer the structural crystallography of $BaCe_{1-x}Ln_xO_{3-\delta}$ [26,27] for a variety of lanthanide dopants. Using factor group analysis, it was concluded that doping with Gd and Yb at $x = 0.05$ left the structure unperturbed from the parent phase; however, doping with Nd gave rise to apparent dopant-concentration-dependent structural phase transitions. For Nd, doping with $x > 0.1$, the number of Raman active modes was found to be consistent with the aristotype phase in space group $Pm\bar{3}m$, and for $0.05 \leq x < 0.1$, the compounds were deduced to be tetragonal with space group $P4/mbm$. Scherban et al. [26] attributed the structural transitions to the substitution or a rare earth with significantly larger ionic radius than Ce^{4+}, and furthermore, Nd^{3+} could be expected to exhibit a Jahn–Teller distortion. Knight and Bonanos concluded that these structural phase transitions were unlikely from crystal–chemical arguments, Nd^{3+} is not a Jahn–Teller ion [28] and the slight change in ionic radius at $x = 0.1$ was unlikely to give rise to the large cooperative rotations of the Ce/NdO_6 octahedra that would be required to move it into the tetragonal stability field. To a good approximation, structural phase transitions in perovskites with rotated octahedra require either temperature or *A*-site substitution (for example, the $Ca_{1-x}Sr_xTiO_3$ solid solution [29]) for significant structural changes to be observed. Initially, Knight and Bonanos [30] investigated $BaCe_{1-x}Nd_xO_{3-\delta}$ for $0.0 \leq x \leq 0.2$ in $x = 0.04$ steps using high-resolution neutron powder diffraction and model-independent fitting. The data were analysed by fitting each data set in turn to all of the 15 possible perovskite space groups that contain at most a single tilt around each pseudocubic axis. The conclusion of this work was unambiguous for $0.0 \leq x \leq 0.16$, Nd does not produce any profound change in the crystal symmetry and the compound remains orthorhombic, space group *Pmcn*, throughout this range. Only for $x = 0.20$ was there any ambiguity in the space group assignment, where the orthorhombic space group *Cmcm* remained a possibility. Knight and Bonanos concluded that structure refinable data were necessary to differentiate between the two space groups at $x = 0.2$. As there is no group–subgroup relationship between the two space groups, any transition that occurred from *Pmcn* to *Cmcm* would have to be first order in doping level and hence, should show up as a distinct discontinuity in the octahedral tilt angles and pseudocubic lattice parameters. These samples were subsequently restudied by Knight [31] using the POLARIS diffractometer at ISIS to determine the effect of doping on the crystal structure. Fig. 6 shows a small part of the final Rietveld refinement for $BaCe_{1-x}Nd_xO_{3-\delta}$ with $x = 0.08$ and 0.16 in the apparent tetragonal and cubic phase fields. For $x = 0.08$, the reflection markers are indexed on the orthorhombic *Pmcn* cell, the italicised indexing is for the tetragonal cell but using *a* as the unique axis rather than *c*. Knight indexed the cell in this non-standard setting for the following reasons. The setting in *Pmcn* has lattice parameters approximately $2a\ \sqrt{2}a\ \sqrt{2}a$, while the standard setting for $P4/mbm$ is $\sqrt{2}a\ \sqrt{2}a\ a$. A transition between these two space groups is permitted by the Landau theory to be second order via the loss of the two antiphase tilt components, and hence, the resulting *c*-axis in the tetragonal phase would have been the *a*-axis in the orthorhombic phase. The character of the superlattice reflections is also shown as *M* or *R*. Note that as the *M*- and the *R*-points are both reciprocal lattice vectors in a phase with space group *Pmcn*, then the reciprocal lattice vector joining them must also be a reciprocal lattice vector. This reciprocal lattice vector is the *X*-point in the pseudocubic Brillouin zone and is the weak feature at ~ 2.45 Å. The principal effect of this mode is a displacement of both the *A*-site cation and the oxygen on the mirror plane. We can see immediately from this figure the advantages that neutron diffraction affords for this kind of analysis in $BaCeO_3$. If the compound had indeed transformed to the tetragonal space group, $P4/mbm$, then the large envelope of *R*-point reflections, as well as the weak *X*-point reflection would have to be absent. In fact, any reflection with odd *h* index in the orthorhombic phase would have to be

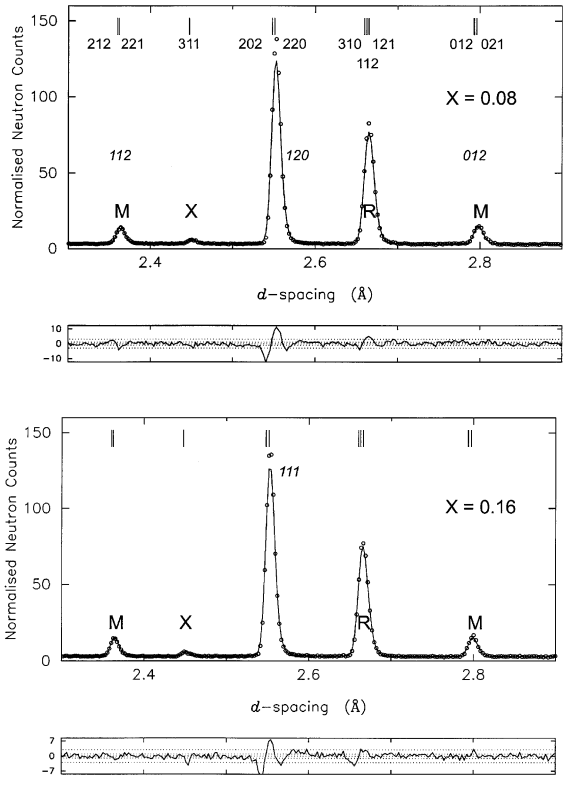

Fig. 6. A comparison of the predicted reflection positions from the space groups inferred from Raman spectroscopy for Ba $Ce_{1-x}Nd_xO_{3-x/2}$ with $x = 0.08$ and 0.16 with the full Rietveld fits in space group *Pmcn*. The superlattice reflections are labelled as arising from either *M*-point or *R*-point tilts. For $x = 0.08$, the Raman data were interpreted as indicating the space group $P4/mbm$, which is indexed in italics for a non-standard setting with *a* as the unique axis. The large *R*-point envelope of reflections should be absent if this space group assignment is correct. For $x = 0.16$, the space group was inferred to be cubic, space group $Pm3m$. In this case, all the superlattice reflections should be absent and only the 111 reflections, in italics, should be observed. The presence of *M*-, *R*- and *X*-point superlattice reflections disprove the Raman space group assignment.

absent in this tetragonal phase as this unit cell parameter would have to halve in length at such a transition. On the basis of the observed superlattice reflections, we have shown that the phase is orthorhombic with space group *Pmcn* for Nd-doping at $x = 0.08$ and is not tetragonal, space group $P4/mbm$.

For the case of $x = 0.16$ in the apparent cubic phase field, we would only expect to see the reflection indexed 111 in italics and all superlattice reflections should be zero. It is clear that all superlattice reflections are visible, and hence, the compound is orthorhombic, space group *Pmcn* for this doping level. While the original refutation of the Raman results utilised the high-resolution diffractometer HRPD, it can be seen from the arguments presented above that the superlattice reflections are well-separated and easily accessible at more modest resolution.

Knight analysed all five data sets using the Rietveld method and found them to be consistent with space group *Pmcn*, and all attempts to refine the $x = 0.2$ sample in *Cmcm* proved to be unsuccessful. Refinement of the site occupancies of the two crystallographically independent oxygen sites showed the

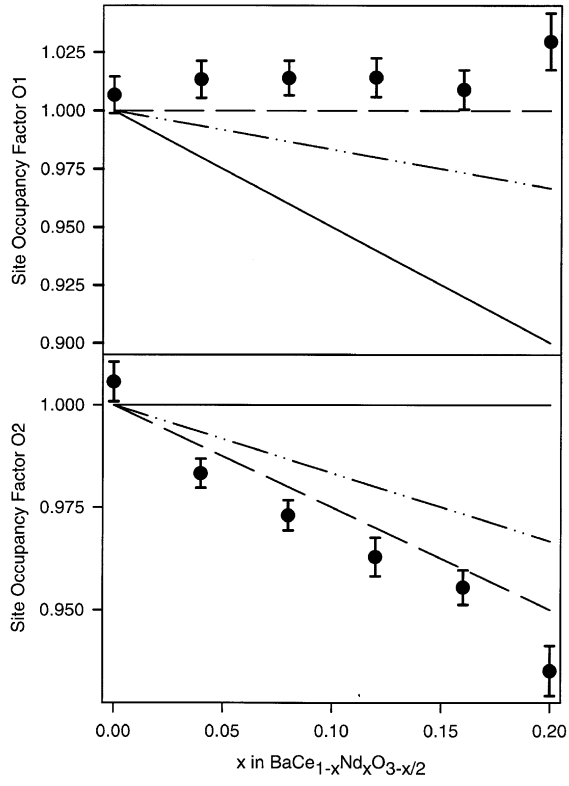

Fig. 7. Comparison of three vacancy ordering models for the extrinsic oxygen vacancy in $BaCe_{1-x}Nd_xO_{3-x/2}$. The full line shows the compositional dependence of the site occupancy factors for the vacancy to be ordered on O_1, which lies on the mirror plane. The dashed line shows the compositional dependence for the vacancy ordering on O_2, and the dot–dash, for the vacancy disordered over both sites. The experimental results support vacancy ordering on the oxygen, O_2, which lies on the general site.

vacancies to be unsaturated throughout the entire compositional range studied. In all cases, the oxygen in the general position showed a site occupancy less than unity, while the oxygen on the mirror plane remained at one within estimated standard deviation. The refinements were then repeated assuming no saturation of the vacancies but included the rigid constraint on the oxygen stoichiometry that this implies. Fig. 7 shows the result of these refinements including a 'free' refinement of the oxygen stoichiometry of $BaCeO_3$ to estimate the reliability of the results. Three simple vacancy models have been evaluated and are shown as lines on the figure; the full line for the vacancy ordered on the oxygen lying on the mirror plane, the dotted line for the vacancy ordered on the oxygen on the general site, and the dot–dash line for the vacancy disordered over both sites. The results clearly support the observation made for the single Y-doped sample that the vacancy orders on to the oxygen in the general equivalent position in the crystal structure.

The results from the structure showed that the average structure, as probed by Bragg diffraction, was barely perturbed by the doping of Nd to $x = 0.2$ refinement (an example of the quality of fit is shown in Fig. 8 for $x = 0.2$). No systematic variation was found for any structural parameter when plotted against dopant concentration, effective *B*-site ionic radius or the variance of the effective *B*-site ionic radius. Additionally, the polyhedral distortion parameters, octahedral volume, octahedral angle variance, and quadratic elongation showed no systematic trends. By way of contrast, the Debye–Waller factors for all atoms showed an increasing linear trend with mol% Nd. Knight attributed this to an additional static disorder component that was additive to the normal thermal vibration and arose from the difference in bonding requirement of Nd^{3+} from Ce^{4+}. However, Knight concluded that diffraction data would need to be collected over wide temperature intervals for a variety of doping levels to verify this hypothesis.

From the neutron powder refinements published so far, there is little evidence for any major perturbation of the parent crystal structure on doping. Transmission electron microscopy studies of these doped materials would be timely to investigate the level and nature of any twinning present, and whether there is any tendency to a long-range ordering of the oxygen vacancies, as has been observed in Ca $Ti_xFe_{1-x}O_{3-x/2}$, a perovskite-brownmillerite solid solution.

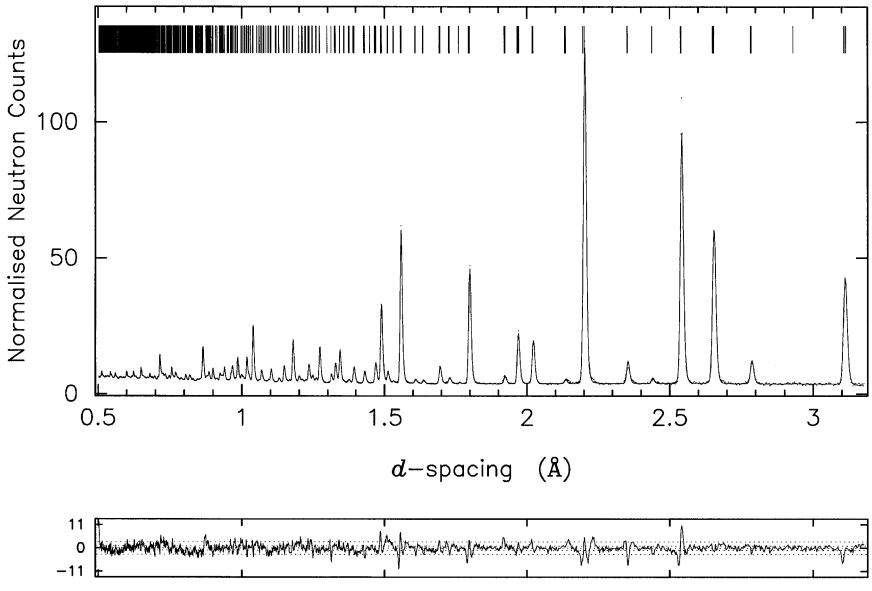

Fig. 8. Rietveld fit to $BaCe_{0.8}Nd_{0.2}O_{2.9}$ in space group *Pmcn*. The observed data are dots, the calculated pattern is shown by the full line. The lower plot shows Δ/σ.

5. High-temperature structural phase transitions

Since the interest generated in the ionic conducting properties of doped $BaCeO_3$, the number, the crystal symmetry, and thermodynamic order of the phase transitions in $BaCeO_3$ has been contentious. In this review, we shall attempt to put the temperature variation of the crystal structure of $BaCeO_3$ on a firm footing using the arguments that have been developed earlier.

The first report of a structural phase transition in $BaCeO_3$ as a function of temperature was made by Preda and Dinescu [17] in a study of the phase relations in the ceria-alkaline earth phase diagrams. Using X-ray diffraction, they found a phase transition at 773 K from a phase they identified as tetragonal to a phase identified as cubic. We have shown earlier that the ambient temperature phase is orthorhombic, and hence, taking into account the low visibility of the superlattice reflections with X-rays, we can discount the structural aspects of this observation. However, the temperature at which the change is observed is close to that determined recently, first by neutron powder diffraction, and later by differential scanning calorimetry. In the first of the recent studies of $BaCeO_3$, the temperature dependence of the Raman spectrum between 298 and 1073 K was made by Scherban et al. [27,32]. Using factor group analysis of Raman active modes, phase transitions from *Pmcn* to $P4/mbm$ at 427 K and $P4/mbm$ to $Pm\bar{3}m$ at 1112 K were inferred. At about the same time, Knight [33] carried out a high-resolution neutron powder diffraction study of $BaCeO_3$ from 298 to 1273 K and found a different sequence of transitions, *Pmcn* to *Incn* at 563 K, *Incn* to $F3\bar{2}/n$ at 673 K and $F3\bar{2}/n$ to $Pm\bar{3}m$ at 1173 K. In the standard settings used in the International Tables for Crystallography, the phases determined by Knight have the following space groups *Pnma*, *Imma*, $R\bar{3}c$ and $Pm\bar{3}m$, respectively. On the basis of the pseudocubic lattice parameters and the volume per formula unit, Knight concluded that the first and last transitions were probably continuous, but the orthorhombic to rhombohedral transition was first order. We shall return to this point later in the article.

The sequence proposed by Scherban et al. was a change from a structure with two equal antiphase tilts and one in-phase tilt, to a structure with a single in-phase tilt, to the aristotype phase. The neutron diffraction data did not support the conclusions of Scherban et al., and to fully disprove the Raman conclusions, Knight [33] used model-independent fitting of his neutron powder data at 473 and 1123 K using their space groups $P4/mbm$ and $Pm\bar{3}m$, respectively. The resultant fits showed large numbers of *R*-point reflections present, but predicted to be zero, for the tetragonal space group, and a smaller number of systematic absent reflections present in the apparent cubic phase field. Despite this conclusive evidence, and the fact that the neutron data gave excellent Rietveld structure refinements in the space groups assigned by Knight, the controversy remained with further publications being made supporting the Raman conclusions [34–37]. As in the case of Nd-doping, we shall use arguments based on superlattice reflections coupled with fundamental line splittings to prove the neutron-assigned space groups.

If the space group changes from *Pmcn* to $P4/mbm$, this will be accompanied by the loss of two antiphase tilts and the *R*-point superlattice reflections will become zero at the phase transition temperature of 427 K. For a phase transition from $P4/mbm$ to $Pm\bar{3}m$, we will lose the single in-phase tilt, and hence, the *M*-point superlattice reflections will go to zero at 1112 K. The top of Fig. 9 shows the summed integrated intensities of a diagnostic *R*-point group of reflections $(310/121/112)$ in black filled circles and the equivalent for a diagnostic *M*-point group of reflections $(012/021)$ with black filled triangles. Both sets are normalised to their integrated intensities at 373 K. It is quite clear from the diagram that the *M*-point reflections become zero at $\sim$ 563 K and the *R*-point reflections at $\sim$ 1173 K. The structural phase transitions therefore, cannot be from *Pmcn* to $P4/mbm$, and the first transition only involves the loss of the single in-phase tilt. In Glazer notation, we have a transition from $a^+b^-b^-$ to $a^0b^-b^-$, which is *Pmcn* to *Incn*, as the unit cell metric remains orthorhombic as confirmed by successful Rietveld refinement. Further evidence for this being the correct transition temperature is afforded by the temperature variation of the pseudocubic lattice constants shown in Fig. 10. The pseudocubic lattice parameters are the lattice parameters of the aristotype phase within the hettotype phase. The calculation of the pseudocubic cell for the phases of

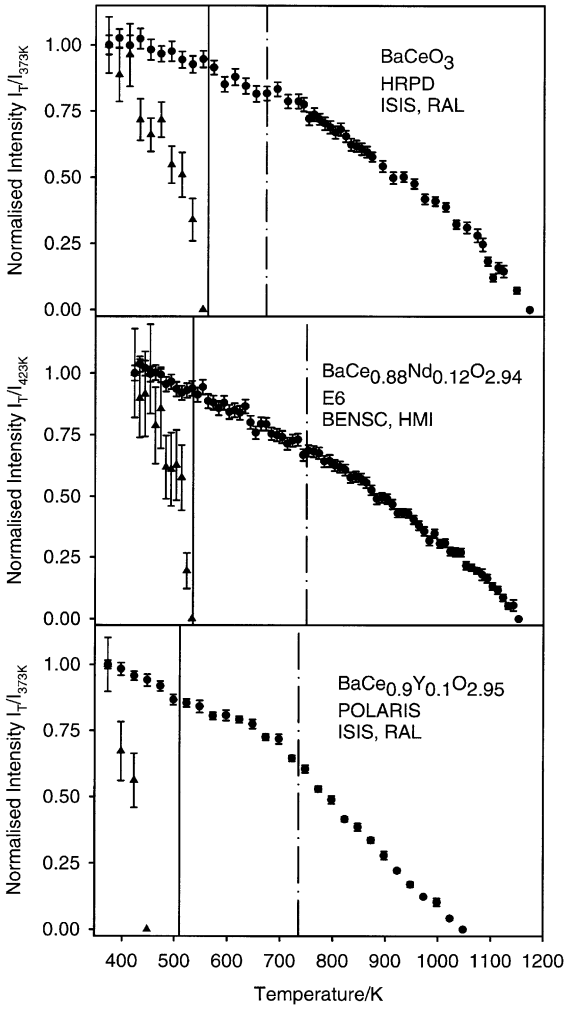

Fig. 9. Normalised intensities for *M*- and *R*-point superlattice reflections as a function of temperature. The in-phase tilts are shown as full black circles and the antiphase tilts as black triangles. The phase boundaries between *Pmcn* to *Incn* and *Incn* to $F3\bar{2}/n$ are shown as vertical solid and dot–dash lines, respectively. The $F3\bar{2}/n$ to $Pm\bar{3}m$ phase boundary occurs when the *R*-point normalised intensity becomes zero. In the case of $BaCeO_3$, the Raman interpretation of the structural phase transitions should show the *R*-point intensities becoming zero at 427 K, and the *M*-point intensities becoming zero at 1112 K. This interpretation is not supported by these data.

$BaCeO_3$ will be given in Appendix A2 of this article; however, it is sufficient to state that in both orthorhombic cells, the pseudocubic cell is monoclinic with $a \neq b = c$, $\alpha \neq 90°$. From the figure, it can be seen that if thermal expansion effects are removed from the data, the pseudocubic cell for the *Pmcn* phase shows a maxima in *b*, *c* and the shear angle α, and exhibits a minima in *a*. Furthermore, it is clear that there is a large discontinuity in the pseudocubic cell and shear angle at 673 K, which was undetectable as a phase change using Raman spectroscopy and which Knight showed to be a phase transition to a rhombohedral cell. As late as 1997, Genet et al. [37] were still disputing the existence of this rhombohedral phase and maintained that the phase was tetragonal $P4/mbm$. We have shown above that this phase cannot be tetragonal, we shall now show it to be rhombohedral.

Fig. 11 shows parts of the diffraction pattern of $BaCeO_3$ collected at 773 K using HRPD. The patterns are indexed according to a doubled cell using the methodologies first suggested by Glazer [6]. From

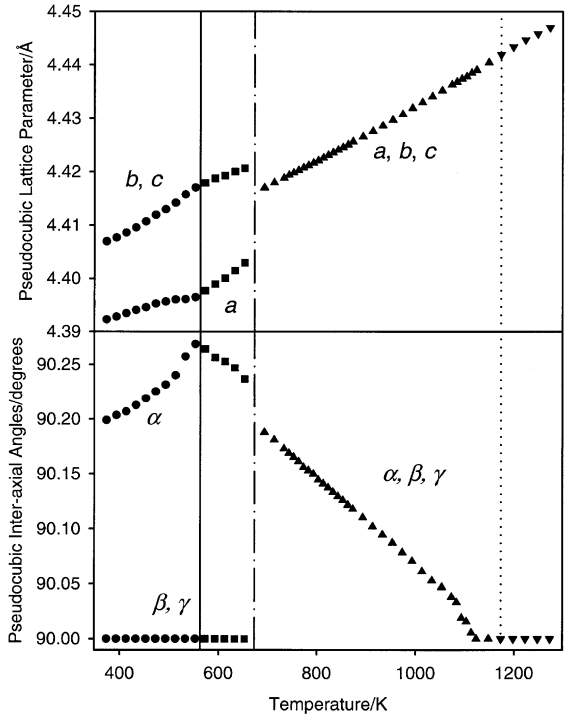

Fig. 10. The pseudocubic lattice constants of $BaCeO_3$. Phase *Pmcn* is shown as black circles, *Incn* as black squares, with the phase boundary being shown as a vertical black line. The first order transition between *Incn* and $F3\bar{2}/n$ is shown by a dot–dash line and the $F3\bar{2}/n$ phase as upward black triangles. The transition to the aristotype is shown by a dotted line, with the $Pm\bar{3}m$ phase as downward pointing black triangles.

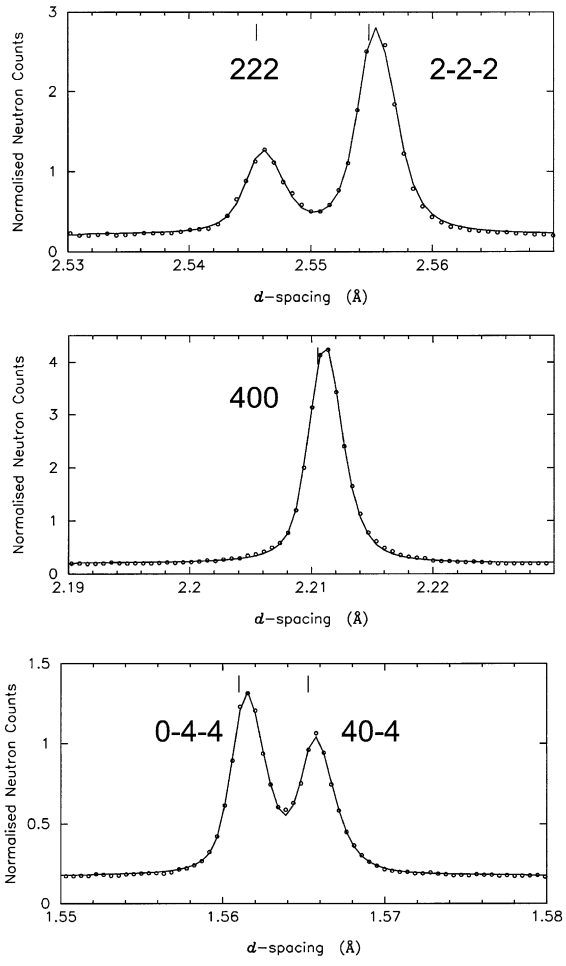

Fig. 11. The diagnostic reflections of $BaCeO_3$ at 773 K proving the rhombohedral metric of the phase below the aristotype.

Fig. 9, we only have *R*-point superlattice reflections in the data, thus limiting the possible space groups to only those that contain at least one minus tilt. Furthermore, if we consider to a good approximation that on descending from the cubic phase, the structure factor amplitudes that were degenerate in the cubic phase will not change significantly on entering the lower temperature phase, we can appeal to the change in multiplicity of these reflections to identify the correct symmetry. From Fig. 11, we can see that the *h00* reflection is unsplit, showing equality of all three pseudocubic axes, while the *hhh* splits approximately in the ratio 3:1 and the *hh0* splits approximately 1:1. We can show that these reflection splittings are entirely consistent with a rhombohedral metric by consideration of the changes in the magnitude of reciprocal lattice vectors that were equivalent in the cubic aristotype.

For a general rhombohedral reflection, *hkl*, the associated reciprocal lattice vector magnitude d^*_{hkl} is

$$d^{*2}_{hkl} = a^{*2}\left(h^2 + k^2 + l^2 + 2(hk + hl + kl)\cos\alpha^*\right)$$

where a^* is the reciprocal lattice vector magnitude and α^* is the reciprocal lattice inter axial angle. If we set $\alpha^* = 90°$, the trigonometric term is zero and we generate the cubic aristotype reciprocal lattice vectors. As the expression for the cubic case only contains the Miller indices in quadratic terms, the signs of the individual Miller index is irrelevant. If we consider the 222 reflections for example, we have eight possible permutations of sign, but all give the same magnitude of d^*_{222}. By contrast, if we consider the case where $\alpha^* \neq 90°$, the sign permutations become important. For 222 and $\bar{2}\,\bar{2}\,\bar{2}$, the inner bracket is positive, for the remaining six permutations, where we have either one positive and two negative, or one negative and two positive Miller indices, the inner bracket is negative. The 222 cubic reflection therefore splits into two separate reflections with multiplicities 2:6, and hence, if we make the assumption of approximate structure factor equality, we expect to see two peaks with an intensity ratio 1:3, as observed in Fig. 11. Furthermore, the order with which the reflections split, i.e. 1:3 or 3:1 with increasing lattice spacing shows whether the direct space interaxial angle, α, is greater or lesser than 90°. In the case of $BaCeO_3$ at 773 K, the intensity ratio is 1:3 with increasing lattice spacing, and hence, the interaxial angle is greater than 90°. For the 400 reflection, the inner bracket is zero, and as the remaining terms are quadratic in the Miller indices, the signs of the individual Miller indices play no part in the determination of the reciprocal lattice vector d^*_{200}. This reflection, therefore, does not split at a cubic to rhombohedral transition as observed. For the 440 reflection, it is easy to see that the 12 contributing reflections fall into two separate classes of six, the first with either two positive or two negative Miller indices, or the second with mixed signs. The resultant, being the cubic reflection, will split into two approximately equal reflections as observed experimentally.

Consideration of Fig. 11 shows that extremely high resolution in the lattice spacings was required to determine the line splittings in $BaCeO_3$ and data collected on POLARIS at ISIS, E6 at HMI and D1b at the ILL [38] all had insufficient resolution to deduce the metric ab initio. However, it is possible to infer the phase transitions at the lower resolution of most neutron powder diffractometers by appealing to the temperature variation of the superlattice reflections. The middle diagram of Fig. 9 shows data collected on $BaCe_{0.88}Nd_{0.12}O_{2.94}$ using the constant wavelength diffractometer E6 at BENSC, HMI and the lowest diagram shows data collected on POLARIS at ISIS for $BaCe_{0.9}Y_{0.1}O_{2.95}$. In the case of the E6 experiment, only data encompassing 43–63° 2θ at a wavelength of 2.382 Å were used to integrate the same pair of diagnostic *M*- and *R*-point reflection envelopes as were used in the HRPD $BaCeO_3$ study. For the POLARIS data, full data sets were collected, but only the same reflections were integrated to determine the temperature variation of the superlattice peaks. It is clear from the figure that the same form of the temperature dependence for the undoped material is observed in the two doped samples with the in-phase tilt being lost first and the antiphase tilt being lost last. Hence, the *Pmcn* to *Incn* transition and the $F3\bar{2}/n$ to $Pm\bar{3}m$ transition are easily inferred from these data. The orthorhombic–rhombohedral phase boundary, which was clear on HRPD as a significant simplification of the diffraction pattern, manifests itself on the POLARIS data as a change in gradient of the *R*-point superlattice peak, and in the E6 data, as a slight change in gradient with, in addition, a small discontinuity of the Bragg angle of the fundamental reflection. These results show that the same structural phase transitions appear in the doped systems as in $BaCeO_3$.

Clearly, the thermodynamic nature of the phase transitions is best answered by calorimetric methods, but on the basis of group-theoretical and -experimental measurements of the temperature dependence of the volume per unit formula, Knight [33] proposed that the first and last transitions were probably continuous and the orthorhombic to rhombohedral had to be first order. This transition occurs between two space groups that are not group–subgroup related, and hence, in the framework of the Landau theory of phase transitions cannot be continuous; furthermore, there is a volume discontinuity of 0.56% per formula unit, phase coexistence over a 20 K interval and a discontinuity in the magnitude of the *R*-point tilt angle. The temperature variation of the octahedral tilt angles in $BaCe_{0.9}Y_{0.1}O_{2.95}$ gives some evidence for the continuous nature of the other two transitions as shown in Fig. 12. Differential scanning calorimetry carried out on $BaCeO_3$ has confirmed Knight's lowest two-phase transition temperatures and their thermodynamic order [39] but similar work on Y- and

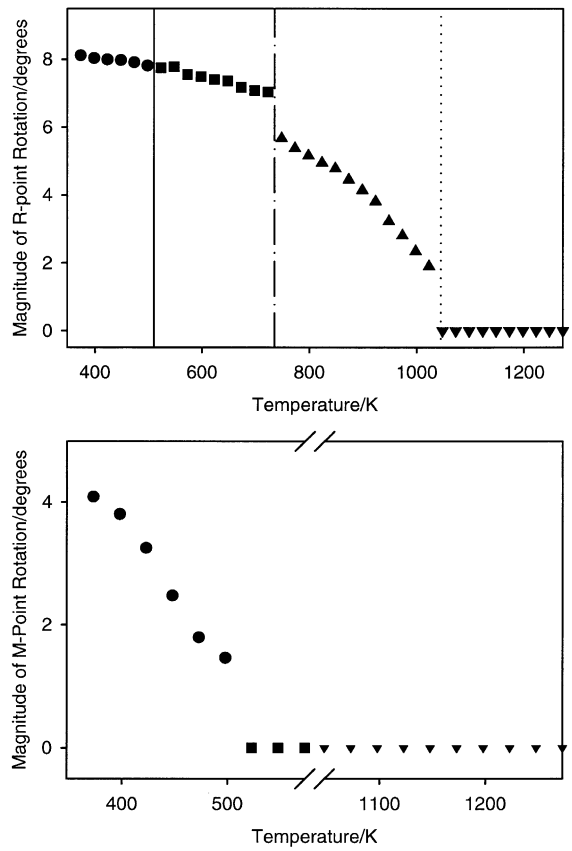

Fig. 12. The magnitudes of the in-phase and antiphase tilts in $BaCe_{0.9}Y_{0.1}O_{2.95}$ derived from full Rietveld structure refinements [45] using the identical symbols as Fig. 10. The near continuity of the *R*-point rotation through the *Pmcn* to *Incn* transition suggests it to be continuous. The first order transition to the rhombohedral phase is clearly seen as a discontinuity in the *R*-point rotation. At the highest temperature transition, these data suggest that the transition may be weakly first order, but the limited resolution on POLARIS made structure refinement closest to the transition temperature difficult and this conclusion needs confirmation by calorimetry.

Nd-doped samples at $x = 0.2$ and 0.1, respectively, were not so clear cut [40]. By contrast, the temperature dependence of the neutron diffraction superlattice reflections for Y-doping at $x = 0.1$ and Nd-doping at $x = 0.12$ prove the existence of these phase transitions.

The lattice parameter data, shown in Fig. 10, have been used in two phenomenological studies of the phase transitions in $BaCeO_3$, the first identifying the magnitudes of the *M*- and *R*-point tilts as the order parameter [41,42], the second using the concept of spontaneous strain [43]. Darlington pointed out that the decrease in the pseudocubic shear angle on entering the *Pmcn* phase from *Incn* implied strong coupling between the *M*- and the *R*-point modes in this phase, but above this transition temperature, the approximate linear behaviour of this shear angle indicated mean-field behaviour. Further, supporting evidence for this mean-field behaviour can be seen in Fig. 9 where the superlattice intensities linearly decrease with increasing temperature. Using a Landau free energy expansion in the magnitudes of the *R*- and *M*-point tilts and the published crystal structures of $BaCeO_3$ in the three non-aristotype phases, Darlington was able to show that coupling coefficients exist that are materials, but not phase-dependent. These coefficients appear to have the same standing as the electrostrictive coupling coefficients as measured on ferroelectric perovskites. Although the rhombohedral–cubic transition has not been measured by DSC, Carpenter gave support to Knight's prediction that the transition was second order by showing the symmetry-adapted shear strain varied linearly with temperature in the range 700–1090 K.

The nature of the phase transitions impacts on supposed single-crystal studies of $BaCeO_3$ in as much as on cooling through the cubic–rhombohedral and rhombohedral to orthorhombic phase transitions, the crystal will inevitably twin. The number of twin domains being related to the quotient of the order of the space groups. Assessment of crystals using transmission electron microscopy is to be recommended if any crystallographic orientational-dependent property is to be measured. Only if the crystal was grown at a temperature below the rhombohedral transition temperature is the probability of twinning reduced.

We have therefore shown that $BaCeO_3$ undergoes a sequence of phase transitions where it first loses an in-phase tilt at 563 K transforming from *Pmcn*, $a^+b^-b^-$, to *Incn*, $a^0b^-b^-$, it then gains a tilt, which is a rare occurrence in perovskites, at 673 K becoming $F3\bar{2}/n$, $a^-a^-a^-$, before finally transforming into the aristotype phase at 1173 K. The effect of doping is not to change the phase transition sequence but does significantly modify the width of the phase fields. For both Y- and Nd-doping, the width of the *Incn* phase is increased over the undoped parent phase and that of the $F3\bar{2}/n$ phase is reduced.

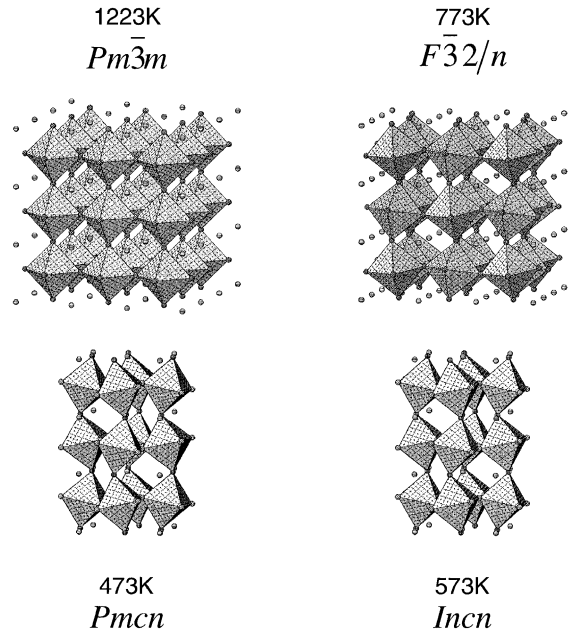

Fig. 13. The crystal structures for the four phases of $BaCeO_3$.

The crystal structures of the four phases of Ba CeO_3 are shown in Fig. 13.

6. Protonation site

The light atom sensitivity of neutron diffraction extends to the proton itself and a structural site for the proton in doped $BaCeO_3$ was proposed by Knight [44] using high-resolution neutron powder data collected on both $BaCe_{0.9}Y_{0.1}O_{2.95}$ and $BaCeO_3$ at 4.2 K. Neutron scattering lengths are isotope-dependent, and Knight pointed out that the optimum experiment would utilise the change in sign of the scattering length for protium- and deuterium-stabilised sam-

ples. In the former case, a negative peak would be observed in the difference nuclear density synthesis, as protium has a negative scattering length of −3.739 fm, and, in the latter case, a positive peak should be found at the same site, as deuterium has a positive scattering length of 6.671 fm. In his study, Knight did not have access to deuterated samples and used the undoped data as a control. Knight argued that at the low proton number densities involved, and in addition the low quality of Fourier maps derived from powder diffraction data, spurious positive and negative peaks in the difference nuclear density synthesis should be expected. Hence, any site found in the doped sample, known to contain structural protons, must be absent in the undoped sample, known to be free of structural protons. Knight found a site in the doped compound, which was stable under Rietveld refinement, and absent in the undoped phase. This site made a chemically sensible O–H bond length of 0.93 Å to oxygen on general positions. No evidence was found for an equivalent site for the oxygen on the mirror plane. Knight concluded that, to be more confident in the structural location of the proton, two criteria had to be satisfied; the first, that a much higher number density of incorporated protons must be achieved, and the second, that only by using the two-isotope method could the results be seen to be truly unambiguous.

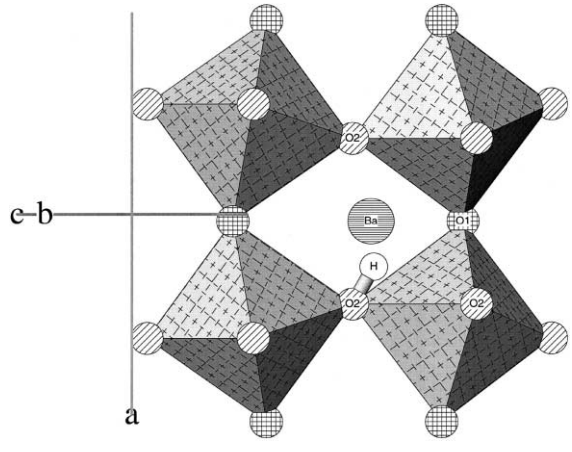

Fig. 14. The proposed structural site for the proton in $BaCe_{0.9}Y_{0.1}O_{2.95}$ at 4.2 K. Additional work using two-isotope exchange is required to verify this structural position.

The proposed position of the proton in $BaCe_{0.9}Y_{0.1}O_{2.95}$ at 4.2 K is shown in Fig. 14.

7. Conclusions

Neutron diffraction has successfully characterised the doped and undoped perovskite $BaCeO_3$ and the main conclusions of this work are summarised below.

(1) At room temperature, $BaCeO_3$ is orthorhombic, with space group *Pmcn* and unit cell $a = 8.777$ Å, $b = 6.236$ Å, $c = 6.216$ Å. The identical space group and axial setting has been found for $BaCe_{0.9}Y_{0.1}O_{2.95}$ and $BaCe_{1-x}Nd_xO_{3-x/2}$ with $0 < x \leq 02$.

(2) Neutron powder diffraction has refuted the structural phase transitions as a function of Nd-doping inferred from Raman spectroscopy.

(3) Crystal structure refinements from neutron powder diffraction data have found the extrinsic vacancy introduced on Y- and Nd-doping to be localised on the oxygen in the general site. The crystal structures of the doped materials show no significant perturbation of the undoped compound.

(4) $BaCeO_3$ undergoes three structural phase transitions between 4.2 and 1273 K. From 4.2 to 563 K, it is orthorhombic, with space group *Pmcn*. At 563 K, it undergoes a second order phase transition to a second orthorhombic phase with space group *Incn*. At 673 K, it undergoes a first order phase transition to a rhombohedral structure with space group $F3\bar{2}/n$. Finally, at 1173 K, it transforms, most probably with a second order phase transition, to the aristotype phase with space group $Pm\bar{3}m$. Y- and Nd-doped samples show the identical sequence, but the widths of the phase fields are modified from the undoped phase. The phase transitions deduced from Raman spectroscopy are not supported.

(5) $BaCeO_3$ single crystals are probably highly twinned due to phase transitions they have experienced on cooling, and hence, any measurement purporting to show directional behaviour requires careful crystal assessment, preferably by transmission electron microscopy.

(6) A chemically sensible site has been proposed for the incorporated structural proton but requires further work for verification.

Table 1
Structural parameters for $BaCeO_3$ at 473 K. Space group: *Pnma*, $a = 6.22714(3)$ Å, $b = 8.79056(4)$ Å, $c = 6.25167(3)$ Å

Atom	*x*	y	z
Ba	0.0123	0.2500	−0.0038
Ce	0.0000	0.0000	0.5000
O_1	−0.0089	0.2500	0.4290
O_2	0.2707	0.0377	0.7302

However, there are still a number of questions which remain unanswered and which neutron diffraction studies, may shed light on.

Providing the vacancies remain unsaturated, neutron diffraction has shown them to be ordered on the oxygen in the general site for Y- and Nd-doping. However, do these vacancies persist at higher temperatures? Knight [33] speculated that if they do up to the rhombohedral phase transition, they must disorder in the rhombohedral phase and proposed that this may be the origin of the increase in the oxide ion transport number at temperatures just higher than this transition temperature. Furthermore, this could explain why doped $SrCeO_3$ does not exhibit appreciable oxide ion conductivity, as it is known not to exhibit any phase transitions between 4.2 and 1273 K [45]. Experimentally, measuring this in doped $BaCeO_3$ is very demanding due to the large Debye–Waller factors associated with the oxygen atoms. It is probably only possible using time-of-flight powder diffraction where the extreme range in *Q* present in the data helps to reduce the correlation between the site occupancy factor and the Debye–Waller factor.

As many laboratories have demonstrated, it is now becoming a routine to stabilise doped $BaCeO_3$ with D_2O, and hence, the two-isotope exchange experiments to locate the structural proton is certainly achievable. These experiments would be possible using any medium-resolution neutron powder diffractometer.

The nature of the phase transitions in Gd-doped $BaCeO_3$ presents a problem to both X-ray and neutron diffraction. We have shown that we were unable to derive a sensible crystal structure for $BaCe_{0.9}Gd_{0.1}O_{2.95}$ using synchrotron X-ray diffraction, and our neutron diffraction data on the same samples were highly compromised by the extreme absorption cross-section of Gd to thermal neutrons. The use of the neutron-transparent isotope ^{160}Gd as a dopant would make these experiments viable and would allow comparison with the data presented here on $BaCe_{0.9}Y_{0.1}O_{2.95}$ and $BaCe_{1-x}Nd_xO_{3-x/2}$.

Finally, the temperature dependence of the Debye–Waller factors on a series of doped samples could shed light on the nature of the static disorder introduced on doping, which we have observed in $BaCe_{1-x}Nd_xO_{3-x/2}$.

Acknowledgements

It is with great pleasure that I acknowledge the technical and scientific help I have received over the past 15 years working on doped $BaCeO_3$ and other perovskites. John Dreyer, Duncan Francis and Chris Goodway are thanked for their help in maintaining the furnaces used in the ISIS experiments, Jimmy Chauhan, Richard Down and Jon Bones for their support in the cryogenic measurements. Steve Hull and Ron Smith aided the experiments on POLARIS as local contacts and Richard Ibberson helped on HRPD. Rainer Sonntag (HMI) is thanked for his hospitality and local contact support on E6 and Michael Hoffmann (HMI) calibrated the wavelength and the resolution function for this instrument. I have learned much about the crystal physics of perovskite phase transitions from discussions with Bill David (ISIS), Ian Wood (UCL), David Price (UCL) and Chris Howard (ANSTO), but mostly from a close collaboration with Nick Darlington (University of Birmingham) over the last 10 years. Of all my collaborators, I am most grateful to Nikos Bonanos (Risø National Laboratory) who first introduced me to the materials science of perovskites, who has synthesised all the samples used in these studies, and

Table 2
Structural parameters for $BaCeO_3$ at 573 K. Space group: *Imma*, $a = 8.79532(4)$ Å, $b = 6.23342(3)$ Å, $c = 6.26224(3)$ Å

Atom	*x*	y	z
Ba	0.0000	0.2500	0.7467
Ce	0.7500	0.2500	0.2500
O_1	0.0000	0.7500	0.8186
O_2	0.7863	0.5000	0.5000

whose interest, ideas and advice have always been appreciated.

Appendix A

A.1. Crystallographic transformations

In the structural work on both doped and undoped $BaCeO_3$, Knight used non-standard settings for all the space groups below the aristotype phase. This, while allowing easy comparison of coordinates between the two orthorhombic space groups, and in addition, the temperature variation of the pseudocubic shear angle throughout the entire temperature interval, did not make the results easily accessible to non-structural workers. The transformations from the non-standard settings to the International Tables for Crystallography are given below.

A.1.1. Pmcn

The standard setting for this space group is *Pnma*, No. 62. The transformation matrix for both the unit cell and the coordinates is given by $001/100/010$.

A.1.2. Incn

An alternative symbol for this space group is *Imam* and the standard setting for this space group is *Imma*, No. 74. In addition to using a non-standard setting, Knight also translated the origin $(1/4, 1/4, 1/4)$ from the standard setting to an alternative centre of symmetry to put the coordinates at the same origin as for the space group *Pmcn*. The transformation matrix for the unit cell and the coordinates is $100/00{-}1/010$. The coordinates of Knight need to have $(1/4, 1/4, 1/4)$ subtracted before transformation.

A.1.3. $F3\bar{2}/n$

The standard setting for this space group is $R3c$, No. 167. The transformation matrix of the unit cell is given by $0\ 1/2\ 1/2\ 1/2\ 0\ 1/2\ 1/2\ 1/2\ 0$ and the coordinates are transformed by the matrix—$111/1\bar{1}1/11\bar{1}$.

Transformed coordinates for $BaCeO_3$ in the standard settings of the space groups at 473, 573 and 773 K are given in Tables 1–3, respectively. Note that the transformed unit cells and fractional coordinates given by Genet et al. [37] based on the results of Knight [33] are incorrect.

Table 3
Structural parameters for $BaCeO_3$ at 773 K. Space group: $R\bar{3}c$, $a = 6.24338(3)$ Å, $\alpha = 60.180(1)°$

Atom	*x*	y	z
Ba	0.2500	0.2500	0.2500
Ce	0.0000	0.0000	0.0000
O	0.1970	0.3030	0.7500

A.2. Pseudocubic transformations

The pseudocubic cells used in this work are for the orthorhombic space groups:

$$\mathbf{a}_p = \mathbf{a}_o/2, \quad \mathbf{b}_p = \mathbf{b}_o/2 + \mathbf{c}_o/2,$$

$$\mathbf{c}_p = -\mathbf{b}_o/2 + \mathbf{c}_o/2, \quad \cos\alpha_p = \mathbf{b}_p \cdot \mathbf{c}_p / b_p c_p$$

and for the rhombohedral space group $F3\bar{2}/n$ setting:

$$\mathbf{a}_p = \mathbf{a}_r/2, \quad \mathbf{b}_p = \mathbf{b}_r/2, \quad \mathbf{c}_p = \mathbf{c}_r/2, \quad \alpha_p = \alpha_r.$$

References

[1] N. Bonanos, K.S. Knight, B. Ellis, Solid State Ionics 79 (1995) 161.
[2] H.D. Megaw, Crystal Structures: A Working Approach. Saunders, Philadelphia, 1973.
[3] W. Cochran, Adv. Phys. 9 (1960) 387.
[4] R.A. Cowley, Phys. Rev. [Sect.] A 134 (1964) 981.
[5] A.M. Glazer, Acta Crystallogr. B 28 (1972) 3384.
[6] A.M. Glazer, Acta Crystallogr. A 31 (1975) 756.
[7] P.M. Woodward, Acta Crystallogr. B 53 (1997) 32.
[8] C.J. Howard, H.T. Stokes, Acta Crystallogr. B 54 (1998) 782.
[9] L.D. Landau, E.M. Lifshitz, Statistical Physics. 3rd edn., Pergamon, New York, 1980.
[10] K.S. Knight, M. Soar, N. Bonanos, J. Mater. Chem. 2 (1992) 709.
[11] K.S. Knight, N. Bonanos, Mater. Res. Bull. 30 (1995) 347.
[12] A. Hoffman, Z. Phys. Chem. B 28 (1935) 65.
[13] E.K. Keler, N.A. Godina, A.N. Kalinina, Zh. Neorg. Khim. 1 (1956) 2556.
[14] A.J. Smith, A.J.E. Welch, Acta Crystallogr. 13 (1960) 653.
[15] E.A. Wood, Acta Crystallogr. 4 (1951) 353.
[16] J.P. Guha, D. Kolar, J. Mater. Sci. 6 (1971) 1174.
[17] M. Preda, R. Dinescu, Rev. Roum. Chim. 21 (1976) 1023.
[18] R.S. Roth, J. Res. Natl. Bur. Stand. 58 (1957) 75.
[19] M. Danelon Mastromonaco, I. Barbariol, A. Cocco, Ann. Chim. (Rome) 59 (1969) 465.

[20] M. Yoshimura, T. Nakamura, T. Sata, Chem. Lett. (1973) 923.
[21] A.J. Jacobson, B.C. Tofield, B.E.F. Fender, Acta Crystallogr. B 28 (1972) 956.
[22] V. Longo, F. Ricciardiello, D. Minichelli, J. Mater. Sci. 16 (1981) 3503.
[23] G.S. Pawley, J. Appl. Crystallogr. 14 (1981) 357.
[24] K.S. Knight, N. Bonanos, J. Mater. Chem. 4 (1994) 899.
[25] W. Münch, K.D. Kreuer, S.T. Adams, G. Seifert, J. Maier, Phase Transitions 68 (1999) 567.
[26] T. Scherban, R. Villeneuve, L. Abello, G. Lucazeau, Solid State Ionics 61 (1993) 93.
[27] T. Scherban, R. Villeneuve, L. Abello, G. Lucazeau, J. Raman Spectrosc. 24 (1993) 805.
[28] M.C.M. O' Brien, personal communication.
[29] C.J. Ball, B.D. Begg, D.J. Cookson, G.J. Thorogood, E.R. Vance, J. Solid State Chem. 139 (1998) 238.
[30] K.S. Knight, N. Bonanos, Solid State Ionics 77 (1995) 189.
[31] K.S. Knight, Solid State Commun. 112 (1999) 73.
[32] T. Scherban, R. Villeneuve, L. Abello, G. Lucazeau, Solid State Commun. 84 (1992) 341.
[33] K.S. Knight, Solid State Ionics 74 (1994) 109.
[34] S. Loridant, L. Abello, E. Seibert, G. Lucazeau, Solid State Ionics 78 (1995) 249.
[35] S. Loridant, G. Lucazeau, Analusis 23 (1995) M17.
[36] G. Lucazeau, L. Abello, Analusis 23 (1995) 301.
[37] F. Genet, S. Loridant, G. Lucazeau, J. Raman Spectrosc. 28 (1997) 255.
[38] F. Genet, S. Loridant, C. Ritter, G. Lucazeau, J. Phys. Chem. Solids 60 (1999) 2009.
[39] V.M. Egorov, Y.M. Baikov, N.F. Kartenko, B.T. Melekh, Yu.N. Filin, Fiz. Tverd. Tela 40 (1998) 2109.
[40] B.T. Melekh, V.M. Egorov, Y.M. Baikov, N.F. Kartenko, Yu.N. Filin, M.E. Kompan, I.I. Novak, G.B. Venus, V.B. Kulik, Solid State Ionics 97 (1997) 465.
[41] C.N.W. Darlington, Phys. Status Solidi A 155 (1996) 31.
[42] C.N.W. Darlington, Phys. Status Solidi B 203 (1997) 73.
[43] M.A. Carpenter, E.K.H. Salje, A. Graeme-Barber, Eur. J. Mineral. 10 (1998) 621.
[44] K.S. Knight, Solid State Ionics 127 (2000) 43.
[45] K.S. Knight, unpublished results.